Editors' Suggestion

High magnetic field ultrasound study of spin freezing in $La_{1.88}Sr_{0.12}CuO_4$

M. Frachet,[1,*] S. Benhabib,[2] I. Vinograd,[1] S.-F. Wu,[1] B. Vignolle,[3] H. Mayaffre,[1] S. Krämer,[1] T. Kurosawa,[4] N. Momono,[5] M. Oda,[4] J. Chang,[6] C. Proust,[2] M.-H. Julien,[1] and D. LeBoeuf[1,†]

[1]*Université Grenoble Alpes, INSA Toulouse, Université Toulouse Paul Sabatier, EMFL, CNRS, LNCMI, Grenoble 38042, France*

[2]*Université Grenoble Alpes, INSA Toulouse, Université Toulouse Paul Sabatier, EMFL, CNRS, LNCMI, Toulouse 31400, France*

[3]*Institut de Chimie de la Matière Condensée de Bordeaux, 33608 Pessac, France*

[4]*Department of Physics, Hokkaido University, Sapporo 060-0810, Japan*

[5]*Muroran Institute of Technology, Muroran 050-8585, Japan*

[6]*Department of Physics, University of Zurich, CH-8057 Zurich, Switzerland*

(Received 29 October 2020; revised 1 February 2021; accepted 26 February 2021; published 18 March 2021)

High-T_c cuprate superconductors host spin, charge, and lattice instabilities. In particular, in the antiferromagnetic glass phase, over a large doping range, lanthanum-based cuprates display a glass-like spin freezing with antiferromagnetic correlations. Previously, sound velocity anomalies in $La_{2-x}Sr_xCuO_4$ (LSCO) for hole doping $p = x \geqslant 0.145$ were reported and interpreted as arising from a coupling of the lattice to the magnetic glass [M. Frachet, I. Vinograd *et al.*, Nat. Phys. **16**, 1064 (2020)]. Here we report both sound velocity and attenuation in LSCO $p = 0.12$, i.e., at a doping level for which the spin freezing temperature is the highest. Using high magnetic fields and comparing with nuclear magnetic resonance measurements, we confirm that the anomalies in the low temperature ultrasound properties of LSCO are produced by a coupling between the lattice and the spin glass. Moreover, we show that both sound velocity and attenuation can be simultaneously accounted for by a simple phenomenological model originally developed for canonical spin glasses. Our results point towards a strong competition between superconductivity and spin freezing, tuned by the magnetic field. A comparison of different acoustic modes suggests that the slow spin fluctuations have a nematic character.

DOI: 10.1103/PhysRevB.103.115133

I. INTRODUCTION

The coupling of electronic instabilities to the crystal lattice plays a significant role in shaping the phase diagram of some high-T_c cuprate superconductors. The case of La-based cuprates is emblematic. Upon cooling, $La_{2-x}Ba_xCuO_4$ (LBCO) and rare-earth doped (Nd, Eu)$_y$-$La_{2-x-y}Sr_xCuO_4$ [(Nd,Eu)-LSCO] evolve from a high-T tetragonal (HTT) to a mid-T orthorhombic (OMT) and finally to a low-T tetragonal (LTT) crystal structure. The LTT order pins stripe order, a combination of mutually commensurate spin and charge modulations, initially found in Nd-LSCO [1]. Within this context sound velocity and attenuation are particularly relevant quantities. Ultrasound measurements directly probe the lattice properties and they are sensitive to any strain-dependent instability.

Among the La-based cuprate family $La_{2-x}Sr_xCuO_4$ (LSCO) appears peculiar. First, the OMT-LTT structural phase transition does not occur, although LTT-like distortions exist locally [2–4]. Moreover, scattering evidence for charge ordering inside the pseudogap phase has remained elusive until recently [5–8]. In LSCO around doping level $p = 0.12$, quasistatic charge modulation appears below $T_{CDW} = 70 \pm 15$ K with a maximal in-plane correlation length $\xi_{\parallel}(T_c) \simeq 30$ Å, a value practically one order of magnitude smaller than in LBCO at the same doping.

In the same compound incommensurate antiferromagnetic (AFM) correlations are also found at low field for $0.02 \leqslant p \lesssim 0.135$ [9]. The temperature at which these correlations appear static depends upon the probe frequency [9,10], revealing the glassy nature of the magnetic state. However, as in other La-based compounds close to $p \approx 0.12$, one observes that the incommensurabilities of charge and spin density waves (CDW and SDW, respectively) follow $2\delta_{spin} = \delta_{charge}$, a relation reminiscent of charge-spin stripe ordering [6].

Close to the hole doping level $p \approx 0.12$ elastic anomalies have been reported in both sound velocity and attenuation. Specifically, in single crystal studies and near the superconducting T_c, a broad sound velocity minimum has been observed in different acoustic modes [11,12]. In a similar range of temperature, an attenuation maximum of longitudinal waves has been found in polycrystals [13,14]. Different interpretations have been proposed to explain this peculiar behavior [11–13,15–17]. Recently, using nuclear magnetic resonance (NMR) and sound velocity measurements in high magnetic field in LSCO for $p \geqslant 0.145$, we showed that the anomalous sound velocity appears to be caused by a coupling of the AFM glass to the lattice [18].

In this study, we strengthen this interpretation with high magnetic field measurements of sound velocity and attenuation in LSCO $p = 0.12$. Comparing ultrasound attenuation

*mehdi.frachet@kit.edu; Present address: IQMT, Karlsruhe Institute für Technologie, 76021 Karlsruhe, Germany.

†david.leboeuf@lncmi.cnrs.fr

with NMR measurements on crystals from the same batch, we reinforce the link between the slowing down of magnetic fluctuations and the ultrasound anomalies observed in the $(c_{11} - c_{12})/2$ and c_{11} elastic constants. Moreover, we show that the ultrasound properties of the $(c_{11} - c_{12})/2$ mode can be semiquantitatively reproduced by a phenomenological dynamical susceptibility model initially developed for canonical spin glasses. Finally, by comparing different acoustic modes, we find that the spin freezing produces an enhanced susceptibility in the B_{1g} channel, which is associated with nematicity in cuprates.

This paper is organized as follows. In Sec. II, we describe the sample studied and the experimental technique. Then, in Sec. III we report the experimental sound velocity and attenuation measurements. We present a phenomenological model of ultrasound in spin glasses and use it to analyze the ultrasound data in Sec. IV. Then, in Sec. V, we discuss the magnetic field effect on the ultrasound properties, the differences between the acoustic modes studied and the symmetry of the AFM fluctuations inferred from our measurements. We summarize our conclusions in Sec. VI.

II. METHODS

A high-quality LSCO single crystal was grown by the traveling solvent floating zone method. From this crystal, three samples were cut along different crystallographic directions to probe different elastic constants. Typical samples dimensions are $2 \times 2 \times 2$ mm^3. The hole doping $p = 0.122 \pm 0.002$ has been determined by measuring $T_{st} = 252$ K, the temperature of the HTT-OMT structural phase transition by sound velocity, as described in Ref. [18]. The different samples share a similar T_{st} and thus a similar doping. The superconducting transition temperature $T_c = 29 \pm 3$ K has been determined by sound velocity, in-plane resistivity, and magnetic susceptibility measurements.

A standard pulse-echo technique with phase comparison was used to measure variations of sound velocity $\Delta v/v$ and sound attenuation $\Delta\alpha$ [19,20]. Ultrasound was generated and detected using commercial $LiNbO_3$ transducers glued onto parallel, clean, and polished surfaces of the samples. The excitation frequency ω ranged from 50 to 300 MHz. For high symmetry propagation direction, the sound velocity variation of a given acoustic mode can be converted to the associated elastic constant change using $\Delta c_{ii}/c_{ii} = 2\Delta v/v$.

Zero-field and static-field experiments were performed at the LNCMI Grenoble using 20 T superconducting and 28 T resistive magnets. Field-cooled conditions were used. Pulsed-fields experiments up to 60 T were carried out at the LNCMI Toulouse. In all cases, the field was applied along the crystallographic c-axis.

III. RESULTS

A. Sound velocity in zero magnetic field

We begin with a zero magnetic-field study of different elastic constants in LSCO $p = 0.12$ as shown in Fig. 1. The description of the different modes studied is reported in Table I. We use a tetragonal representation for the elastic constants even in the OMT phase since the sample is in a

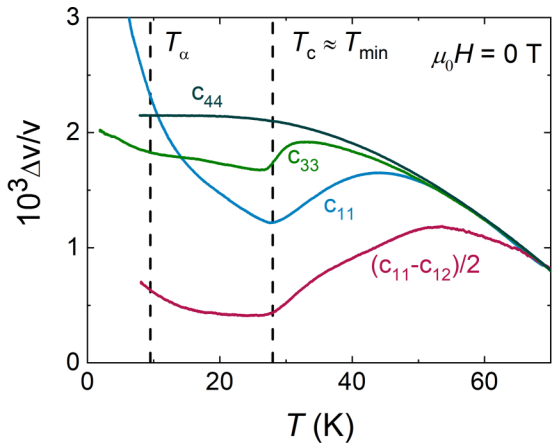

FIG. 1. Sound velocity variation $\Delta v/v$ as a function of temperature for different acoustic modes as indicated. No magnetic field is applied, the curves are arbitrarily superimposed at $T = 70$ K. T_{min} refers to the minimum in the c_{11} elastic constant that coincides with the superconducting T_c in zero magnetic field. T_α indicates the spin freezing temperature at the μeV ultrasound energy scale, defined by an attenuation peak (see Fig. 2). $\Delta v/v$ is calculated with reference value at $T \approx 60$ K.

pseudotetragonal lattice [21]. The c_{44} acoustic mode follows the classical variation expected in solids: upon cooling the sound velocity increases continuously and eventually saturates at low temperature [22]. This behavior contrasts with the c_{33} elastic constant which shows a downward jump at T_c. This mean-field anomaly at the superconducting transition is expected for a longitudinal mode and is related to the specific heat jump through the Ehrenfest relationship

$$\Delta c_{ii}(T_c) = -\frac{\Delta C_p(T_c)}{V_{mol} T_c} \left(\frac{dT_c}{d\epsilon_i} \right)^2, \quad (1)$$

with $\Delta C_p(T_c)$ the specific heat jump at T_c and V_{mol} the molar volume. The amplitude of the anomaly $\Delta v/v(T_c) \simeq 0.2 \times 10^{-3}$ is consistent with literature values on samples with similar doping levels [21,23].

For $T \geqslant T_c$, the temperature dependence of c_{11} and $(c_{11} - c_{12})/2$ elastic constants is remarkable. In both of these modes, the normal state sound velocity decreases upon cooling, until the temperature hits T_c where it shows an upturn. Consequently, the sound velocity in these modes has a minimum at $T_{min} \simeq T_c$. Figure 1 shows that the anomalous lattice softening appears only in acoustic modes having a B_{1g} strain compo-

TABLE I. Properties of the different elastic constants measured: direction of propagation ($\vec{k}$) and polarization ($\vec{u}$) of the acoustic wave, strain (ϵ_{ij}), and associated symmetry. The indices of elastic constants are expressed in the Voigt notation. Crystallographic directions are those of the HTT phase (D_{4h} point group).

c_{ij}	$\vec{k}$	$\vec{u}$	ϵ_{ij}	symmetry
c_{11}	[100]	[100]	ϵ_{xx}	$A_{1g} + B_{1g}$
c_{33}	[001]	[001]	ϵ_{zz}	A_{1g}
c_{44}	[100]	[001]	$\epsilon_{yz}, \epsilon_{zx}$	E_g
$(c_{11} - c_{12})/2$	[110]	[1$\bar{1}$0]	$\epsilon_{xx} - \epsilon_{yy}$	B_{1g}

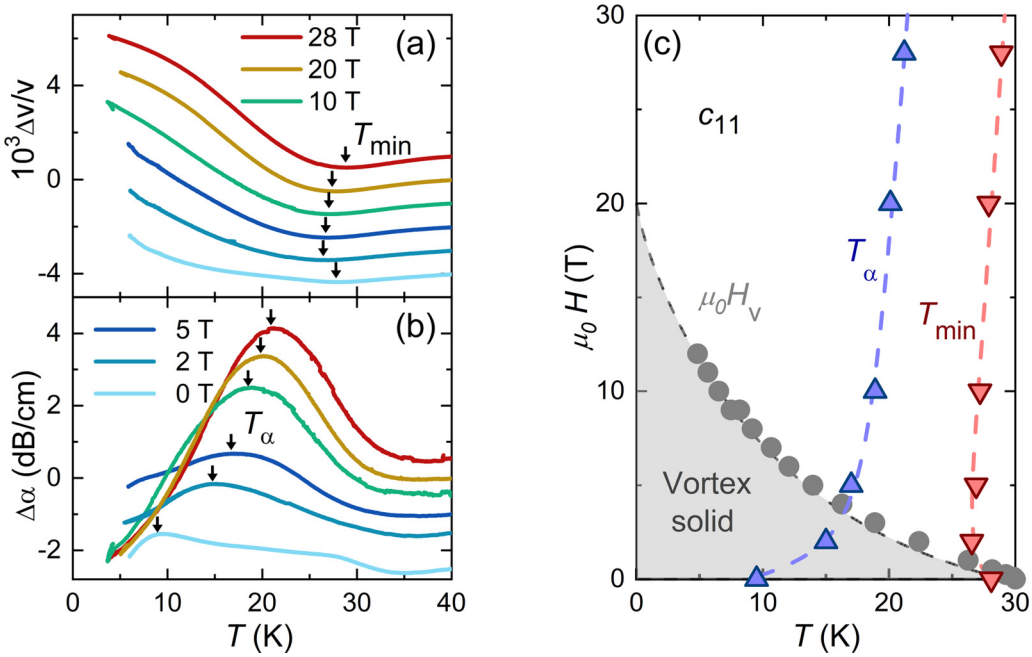

FIG. 2. Static field ultrasound measurements in the c_{11} acoustic mode up to 28 T. (a) $\Delta v/v$ and (b) $\Delta\alpha$ as a function of temperature for different magnetic fields. The curves are shifted vertically for clarity. Reference value taken at $T \approx 30$ K. The arrows denote T_{min} and T_α as indicated. (c) H–T phase diagram: gray circles denote the vortex melting transition field $\mu_0 H_v$ inferred from in-plane resistivity $\rho(T)$ measurements [95% resistivity drop with respect to $\rho(T = 50\,\mathrm{K})$], T_α (upward-pointing blue triangles) and T_{min} (downward-pointing red triangles) refer to the maximum in attenuation and minimum in velocity, respectively. Error bars are smaller than the symbol size. Dashed lines are guides to the eye.

nent, namely c_{11} and $(c_{11} - c_{12})/2$. Note that, so far, we have not been able to measure the B_{2g} mode (c_{66}) for $T < T_{st}$.

Finally, for $T \lesssim 15$ K or so, a rapid stiffening is observed in c_{11} upon cooling. Indeed, the sound velocity in the $T = 0$ limit greatly exceeds what would be expected from an extrapolation of the high-temperature bare elastic constant (e.g., following the c_{44} elastic constant). A similar upturn is found in c_{33} and $(c_{11} - c_{12})/2$ upon cooling for $T \lesssim 15$ K, although much weaker than in c_{11}.

B. Sound velocity and attenuation in applied magnetic field

In Figs. 2 and 3 we investigate how the anomalous sound velocity, and the corresponding sound attenuation, evolve as a function of temperature at different magnetic fields, in the c_{11} and $(c_{11} - c_{12})/2$ modes, respectively. In both these modes no signature of the vortex lattice is observed, as discussed in Appendix A.

The anomalous features of the zero field sound velocity in the c_{11} and $(c_{11} - c_{12})/2$ acoustic modes are enhanced by a magnetic field: both the amplitudes of the lattice softening (for $T \geqslant T_{min}$) and stiffening ($T \leqslant T_{min}$) increase with increasing magnetic field. For both acoustic modes an attenuation peak is found at $T_\alpha \leqslant T_{min}$. The amplitude of this attenuation peak and T_α increase monotonically with increasing field.

The magnetic field dependencies of T_α and T_{min} from c_{11} measurements are shown in the phase diagram of Fig. 2(c). Within error bars, $(c_{11} - c_{12})/2$ and c_{11} show at a given magnetic field similar T_α and T_{min}. In contrast with T_α, T_{min} has a nonmonotonic field dependence: it decreases for $0 \leqslant \mu_0 H \leqslant 2$ T and increases for higher fields. The initial decrease is

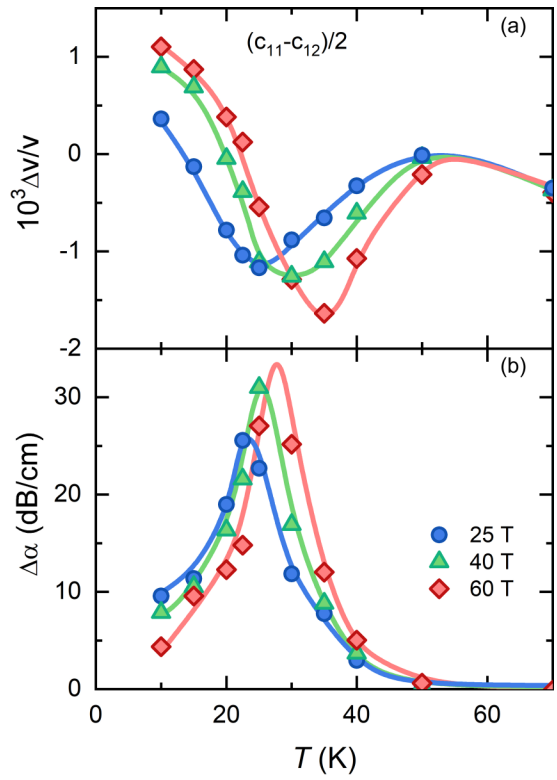

FIG. 3. Temperature dependence of the $(c_{11} - c_{12})/2$ acoustic mode in pulsed-fields up to 60 T. (a) $\Delta v/v$ and (b) $\Delta\alpha$ both extracted from fixed magnetic field cuts of the pulsed-fields isotherms to which we add the zero field curve. Data are relative to value at $T \approx 40$ K. All lines are guides to the eye.

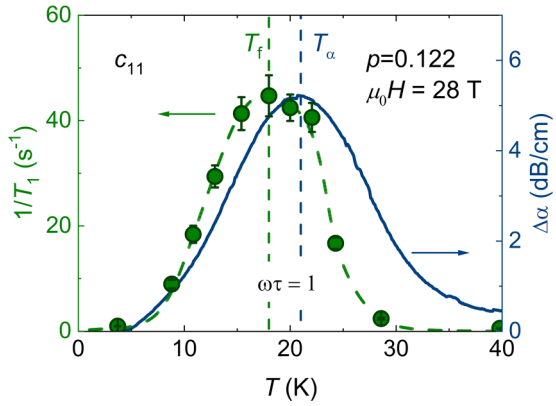

FIG. 4. Comparison between the ultrasound attenuation $\Delta\alpha$ (blue line, right scale) and the ^{139}La NMR spin-lattice relaxation rate $1/T_1$ (green circle, left scale), at $\mu_0 H = 28\,\mathrm{T}$. NMR and ultrasound samples are from the same batch. Both physical quantities show a peak when the excitation frequency becomes equal to the frequency of the spin fluctuations, i.e., $\omega\tau = 1$. A phenomenological linear background has been subtracted from the experimental $\Delta\alpha$ for clarity. The dashed green line is a guide to the eye.

caused by the lattice coupling to the superconducting order parameter as further detailed in Appendix B. However, for $\mu_0 H \geqslant 5\,\mathrm{T}$ or so, the two temperature scales have similar field dependence, indicating that they are coupled and caused by the same phenomenon.

C. Comparison with NMR $1/T_1$

In Fig. 4 we compare the ultrasound attenuation $\Delta\alpha$, with the ^{139}La NMR spin-lattice relaxation rate $1/T_1$ both measured in LSCO $p = 0.12$ samples from the same batch and in a magnetic field $\mu_0 H = 28\,\mathrm{T}$. The comparison is striking, both quantities display remarkably similar temperature dependencies and show a maximum at comparable temperatures.

The peak in $1/T_1$ is a classical signature of spin freezing in superconducting LSCO [24–27]. This peak is understood within the so-called Bloembergen-Purcell-Pound (BPP) model [24,27,28] originating from a diverging correlation time $\tau(T)$. Upon cooling, spin fluctuations are gradually slowing down. At the temperature where the condition $\omega_{\mathrm{NMR}}\tau = 1$ is fulfilled (ω_{NMR} being the NMR frequency), $1/T_1$ is maximum. This temperature defines the freezing temperature T_{f} at the NMR timescale. Notice that the peak in $1/T_1$ is of magnetic origin (i.e., it does come from fluctuations of the electric field gradient) for several reasons: the values of ^{139}La $1/T_1$ for the low T peak are much shorter than for the structural HTT-OMT transition [18,29], the concomitant wipeout of the ^{63}Cu signal is quantitatively explained by magnetic relaxation due to slow spin fluctuations [27,30] and the NMR peak temperature matches well the spin freezing temperature measured by muon spin rotation data across the phase diagram [9,24,31].

Figure 4 reveals that the ultrasound attenuation $\Delta\alpha$ is governed by a similar correlation time. At the temperature where the condition $\omega_{\mathrm{US}}\tau = 1$ is met, with ω_{US} the ultrasound frequency, a peak in the ultrasound attenuation is observed. The good agreement between T_{f} and T_α is provided by the fact that $\omega_{\mathrm{NMR}} \approx \omega_{\mathrm{US}} \approx 10^8$ Hz. Finally, note that the small difference observed between $\Delta\alpha$ and $1/T_1$ could arise from a small variation in doping level between the two samples, but also from a disparity in the way these probes couple to the magnetic moments. This is discussed in the next section.

IV. MODELING

A broad sound velocity minimum at T_{min} [32–34] and an attenuation peak at $T_\alpha \leqslant T_{\mathrm{min}}$ [32,35] are common characteristics of—insulating or metallic—canonical spin glasses around the spin freezing temperature. The sound velocity and attenuation of a cobalt fluorophosphorate spin glass shown in Fig. 5(a) exemplify those features. The comparison with the elastic properties of LSCO $p = 0.12$ in the $(c_{11} - c_{12})/2$ mode shown in Fig. 5(b) is striking: both systems show remarkably similar phenomenology.

In the following, we focus on the transverse $(c_{11} - c_{12})/2$ acoustic mode shown in Fig. 3 and demonstrate that it can be semiquantitatively reproduced by a phenomenological model developed for spin glasses. The strong increase observed in $c_{11}(T)$ at low temperature is not explained by this model and will be discussed later.

We use the phenomenological dynamical susceptibility model developed by Doussineau *et al.* [32,36]. Sound velocity and attenuation are expressed in terms of a complex elastic constant, $c(\omega, T)$:

$$c(\omega, T) = c_0[1 - g^2\chi_4(\omega, T)]. \tag{2}$$

With c_0 the bare elastic constant, g the spin-phonon coupling constant, and ω the ultrasound measurement frequency. Ultrasound quantities are deduced through

$$\Delta v/v = \frac{1}{2}\mathrm{Re}(\Delta c/c), \tag{3}$$

$$\Delta\alpha(\mathrm{dB/cm}) = \frac{\omega}{v}\frac{10}{\log(10)}\mathrm{Im}(\Delta c/c). \tag{4}$$

Here $\chi_4(\omega, T)$ is a dynamical susceptibility defined as

$$\chi_4(\omega, T) = \int \frac{d\tau_4}{\tau_4}\frac{\chi_4(\omega = 0, T)}{1 + i\omega\tau_4}, \tag{5}$$

where $\chi_4(\omega = 0, T)$ is a static susceptibility and $\tau_4(T)$ is the correlation time of the spin fluctuations. In our case, since we are presumably dealing with spin-1/2 Cu^{2+} moments, the magnetoacoustic coupling arises from the Waller mechanism (also called the exchange-striction mechanism), i.e., a modulation of the exchange interaction by the strain [37]. Consequently, the associated susceptibility is quadrupolar and the correlation time is involved in a four-spin correlation function. In contrast, the $1/T_1$ NMR relaxation rate is governed by a correlation time $\tau_2(T)$ which is involved in a two-spin correlation function. This can produce slight differences between $\Delta\alpha$ and $1/T_1$ in Fig. 4 [38]. We use the following expressions for $\tau_4(T)$ and $\chi_4(\omega = 0, T)$:

$$\tau_4(T) = \tau_\infty \exp(E_0/T), \tag{6}$$

$$\chi_4(\omega = 0, T) = \chi_0 + \frac{C_{\mathrm{curie}}}{T}. \tag{7}$$

C_{curie} controls the amplitude of the lattice softening for $T \geqslant T_{\mathrm{min}}$, E_0 is an energy scale that governs T_{min} and T_α, χ_0

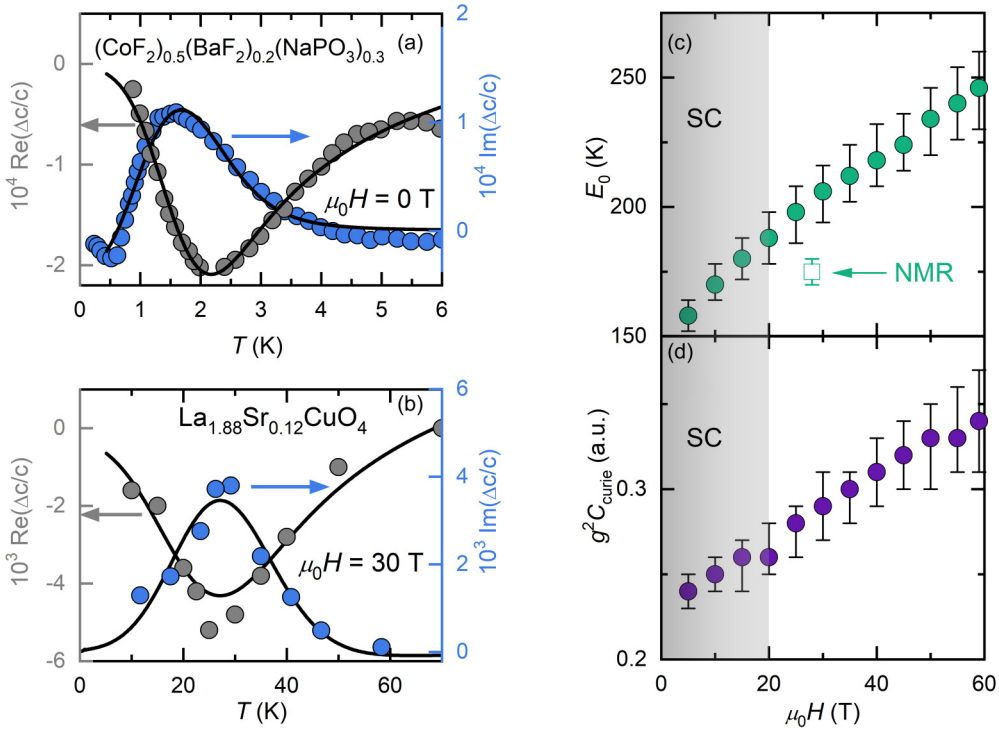

FIG. 5. Fitting of the experimental $\mathrm{Re}(\Delta c/c)$ (gray circles, left scale) and $\mathrm{Im}(\Delta c/c)$ (blue circles, right scale) for (a) the cobalt fluorophosphorate canonical spin glass in a longitudinal acoustic mode reproduced from Ref. [32] and (b) LSCO $p = 0.12$ at $\mu_0 H = 30\,\mathrm{T}$ in the $(c_{11} - c_{12})/2$ transverse mode. In panels (a) and (b) a background sound velocity was subtracted. The black lines are fit to the data using the dynamical susceptibility model. Fitting parameters for cobalt fluorophosphate are $E_0 \approx 18\,\mathrm{K}$ and $g^2 C_{\mathrm{curie}} \approx 10^{-3}$ a.u. Fitting parameters for LSCO $p = 0.12$ are shown in panels (c) E_0 and (d) $g^2 C_{\mathrm{curie}}$. The other two free parameters, $g^2\chi_0 \approx -4.5$ a.u. and $\Delta E_0 \approx 70\,\mathrm{K}$, do not show any significant field dependence. For comparison E_0 extracted from NMR $1/T_1$ at 28 T found in Fig. 4 (empty square) is also shown. The error bars on a single parameter are estimated by monitoring the error of the fit with all other parameters fixed.

is the constant term of the susceptibility and finally τ_∞ is the correlation time of spin fluctuations for $T \gg E_0$. Note that Eqs. (6) and (7) are motivated by an analysis of ^{139}La NMR $1/T_1$ [24,27] and ac-susceptibility measurements in the AFM glass of LSCO [39,40], respectively. As inferred from various experiments [41], the value of τ_∞ is fixed to $\exp(-30) \simeq 10^{-13}$ s. Moreover, as usually done in spin glasses [32,42], and especially in the AFM glass phase of LSCO [27,41], we consider that $\tau_4(T)$ is inhomogeneous using a Gaussian-distribution of E_0 with full width at half maximum $2\Delta E_0$. Within this framework it is possible to fit simultaneously $\Delta v/v$ and $\Delta\alpha$, and to extract both E_0 and $g^2 C_{\mathrm{curie}}$ as a function of a magnetic field. A representative example is shown on Fig. 5(b): the model reproduces most of the salient features seen in the two ultrasound quantities.

The evolution of the fitting parameters is shown in Figs. 5(c) and 5(d). Up to $\mu_0 H = 60\,\mathrm{T}$—i.e., well above our $T \to 0$ extrapolation of the vortex melting field H_{v} on Fig. 2(c)—E_0 and $g^2 C_{\mathrm{curie}}$ increase continuously. The increase of E_0 is related to the nonsaturating values of the temperature scales T_α and T_{min}. Regarding the raise of $g^2 C_{\mathrm{curie}}$, it is explained by the continuous increase of the amplitudes of the lattice softening and attenuation peak up to 60 T (see Fig. 3).

The NMR $1/T_1$ data at $\mu_0 H = 28\,\mathrm{T}$ shown in Fig. 4 can be fitted with the BPP formula using Eq. (6) for $\tau_2(T)$ and a Gaussian distribution of activation energy E_0 [27,43]. This parametrization of $1/T_1$ data yields an activation energy in fair agreement with E_0 inferred from ultrasound data [see Fig. 5(c)]. It has been suggested previously that the activation energy is analogous to the spin-stiffness $2\pi\rho_s$ [25,43,44]. The value of $E_0 \approx 200\,\mathrm{K}$ found here for $\mu_0 H = 20\,\mathrm{T}$ is comparable to what is obtained in Nd-LSCO $x = 0.12$ in zero magnetic field [25,44,45]. It is an order of magnitude smaller than the spin stiffness of the antiferromagnetic parent compound La_2CuO_4 where $2\pi\rho_s \approx J$ [46].

Finally, in the paramagnetic state of a classical Néel AFM $C_{\mathrm{curie}} \propto \mu^2$, where μ is the magnetic moment. Since the dynamical susceptibility model is purely phenomenological, we cannot extract microscopic information. As such, the increase of $g^2 C_{\mathrm{curie}}$ with magnetic field [see Fig. 5(d)] could originate from an enhanced μ [47,48] or from an increased magnetic volume [31].

V. DISCUSSION

Let us summarize our results so far. (i) The $(c_{11} - c_{12})/2$ and c_{11} modes show a softening for $T \geqslant T_{\mathrm{min}}$ and a hardening for $T \leqslant T_{\mathrm{min}}$. Those features are enhanced by magnetic field and survive when superconductivity is strongly suppressed by the field. Consequently, neither feature is caused by superconductivity. We attribute this broad sound velocity minimum to the freezing of the AFM glass. (ii) The striking similarity of the ultrasound attenuation with the NMR relaxation rate $1/T_1$ shows that the AFM glass is also causing the anomalous

attenuation peak in high magnetic field. (iii) The behavior of the $(c_{11} - c_{12})/2$ elastic constant found in LSCO $p = 0.12$ in high magnetic field is remarkably similar to what is found in canonical spin glasses. A dynamical susceptibility model, developed in the context of spin glasses, reproduces all features of the anomalous ultrasound properties in the $(c_{11} - c_{12})/2$ mode.

The similar decrease of $T_{\rm min}$ and T_c with magnetic field $\mu_0 H \leqslant 14\,$T in LSCO at $p \approx 0.14$ has previously motivated a scenario in which a competing lattice instability—that produces a lattice softening for $T > T_c$—is quenched by the onset of superconductivity that induces a hardening for $T < T_c$ [12]. While we observe the same behavior in LSCO $p = 0.12$ for $\mu_0 H \leqslant 2\,$T (see Appendix B for more details), this scenario does not hold at higher field where we observe an increase of $T_{\rm min}$. All measurements reported here in LSCO $p = 0.12$ support the interpretation that the ultrasound anomalies are caused by the AFM glass phase via spin-phonon coupling [18].

In the following we discuss some implications of the aforementioned results. In particular, we comment on the magnetic field effect on the ultrasound properties, the relation of this study with previous elastic experiments and the symmetry of the AFM quasistatic fluctuations.

A. Special coupling with B_{1g} strain

In canonical spin glasses such as cobalt fluorophosphorate, the magnetic moments are frozen in a random manner. Consequently, longitudinal and transverse acoustic modes couple similarly to the spins in such systems (see Ref. [36]). The magnetic moments of LSCO have similar dynamical properties as canonical spin glasses: they gradually freeze as the system is cooled down, such that the onset temperature depends on the probe frequency [9,10]. However, the moments in LSCO arrange in a pattern displaying incommensurate AFM character, and Bragg peaks indicating correlation lengths as high as ~200 Å in LSCO $x = 0.12$ are observed in neutron diffraction experiments [47,49–51]. Consequently, in LSCO the coupling between the frozen spins and the lattice varies dramatically from one mode to another, as shown in Fig. 1. The anomalous softening for $T \geqslant T_{\rm min}$ is observed only in modes transforming according to the B_{1g} irreducible representation (see Table I and Fig. 1). Note, however, that we cannot exclude a similar coupling of the AFM glass to B_{2g} mode. Nonetheless, this suggests a special role of the B_{1g} mode.

Within the framework of the dynamical susceptibility model, the lattice softening in the B_{1g} mode is caused by the growth of a Curie-like susceptibility $\chi_4(\omega = 0, T)$. Equation (2) is reminiscent of the elastic constant $c = d^2F/d\epsilon^2$ calculated using a Landau free energy F containing a bilinear coupling $F_c = g\epsilon Q$ [52], with ϵ a strain and Q an order parameter. Indeed, within such a model, the softening is directly related to the increasing mean-field susceptibility of Q, $\Delta v/v \propto -g^2\chi_Q$. For this bilinear coupling to exist, both ϵ and Q must transform according to the same irreducible representation. In this context, our result would suggest that the order parameter (and the fluctuations) associated with the AFM glass has a B_{1g}, i.e., nematic, character.

Although conjectural in the absence of a measurement of the B_{2g} mode, this interpretation of the ultrasound data is evocative of the B_{1g} susceptibility observed by symmetry-resolved Raman scattering in LSCO at $x = 0.10$ [53]. It is consistent with evidence of charge and spin stripe orders in this compound [6,51,54,55]. Nematicity can indeed result from fluctuating stripes [56]. We note that, at $p \sim 0.12$, the B_{1g} susceptibility develops for $T \leqslant 70\,$K, well below the pseudogap temperature $T^\star \approx 130\,$K [57]. The lack of B_{1g} susceptibility at the pseudogap temperature is also reported in symmetry-resolved electronic Raman scattering experiments in $Bi_2Sr_2CaCu_2O_{8+\delta}$ [58]. The onset temperature of our detection of B_{1g} susceptibility is actually comparable to the CDW onset temperature $T_{\rm CDW} = 70 \pm 15\,$K [5–7]. This suggests that, in LSCO $p = 0.12$, charge-stripe order triggers slow magnetic fluctuations [29,59,60] with nematic character.

B. Effect of the magnetic field

Previous neutron scattering and μSR experiments have shown that the magnetism of LSCO at $p \approx 0.12$ is enhanced by a magnetic field [47,48,61–64], and this effect has been ascribed to a competition between superconducting and AFM order parameters. In line with this interpretation, we observe that the ultrasound signatures of the AFM glass are strengthened by a magnetic field (see Figs. 2, 3, and 5). The magnetic field dependence of the ultrasound properties does not saturate up to 60 T and the magnetic-field-induced softening appears at temperatures as high as $T \approx 50\,$K (see Fig. 3). These observations are puzzling since at this doping $T_c \approx 29\,$K and the extrapolation of the vortex melting line leads to $\mu_0 H_v(T \longrightarrow 0) \approx 20\,$T. This raises important questions on the effect of magnetic fields on the magnetic freezing and the possible resilience of superconducting fluctuations in high field.

We note that this behavior is reminiscent of the magnetoresistance producing an upturn in the resistivity of superconducting LSCO in high fields. This magnetoresistance is observed up to $T \simeq 100\,$K at the doping level $p = 0.12$ [65]. The spin freezing has been previously discussed as a cause of the resistivity upturn in La-based cuprates [66–70]. Consequently, it is possible that the large magnetoresistance observed in LSCO $p = 0.12$ above T_c is related to the field-induced gradual slowing down of magnetic fluctuations observed here.

C. Differences between c_{11} and $(c_{11} - c_{12})/2$

Finally, we discuss the differences between the c_{11} and $(c_{11} - c_{12})/2$ modes. As discussed above, the strength of the magnetoacoustic coupling is largest in the $(c_{11} - c_{12})/2$ mode, where the largest softening is observed (see Fig. 1). The second difference between the response in these two modes is the field-enhanced hardening that is seen in c_{11} at low temperature. The situation is schematically depicted in Fig. 6. In the $(c_{11} - c_{12})/2$ mode, the difference between the measured sound velocity in the $T \to 0$ limit and the background velocity is negligibly small. On the other hand, this difference is significant in the c_{11} mode, with the measured sound velocity being larger than the background velocity. This behavior echoes the results from previous studies performed

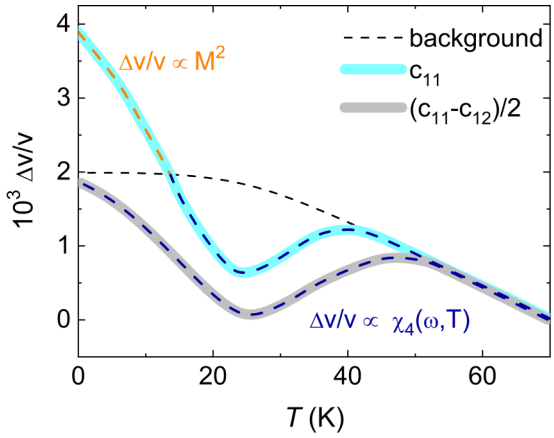

FIG. 6. Schematic representation of the sound velocity of the $(c_{11}-c_{12})/2$ (gray) and c_{11} (cyan) modes in LSCO $p=0.12$. Black dashed line is the background elastic constant arising from the anharmonicity of the ionic potential [22]. $(c_{11}-c_{12})/2$ can be fully reproduced by the dynamical susceptibility model involving $\chi_4(\omega,T)$ (dashed blue line). For $T\to 0$, the difference between the sound velocity of the $(c_{11}-c_{12})/2$ mode and its background tends to zero. This contrasts with the behavior of c_{11}. For $T\to 0$, the sound velocity of the c_{11} mode is larger than the background sound velocity. This means that in addition to the contribution from $\chi_4(\omega,T)$ (dashed blue line) that causes the minimum in c_{11}, another component contributes at low T. As discussed in the text, a contribution proportional to M^2 (dashed orange line) could explain the rapid increase of c_{11} at low temperature.

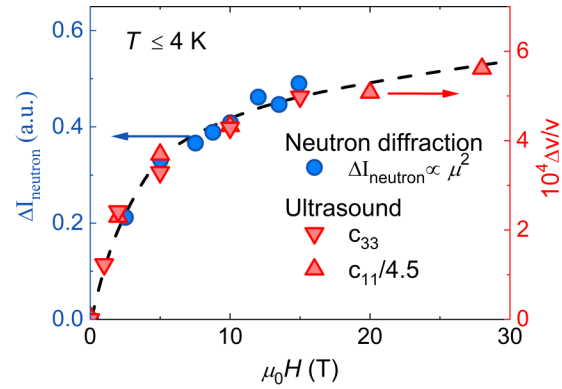

FIG. 7. Comparison between the magnetic field dependence of the superlattice Bragg peak intensity of incommensurate AFM seen by neutron diffraction, $\Delta I_{neutron}$ (blue circles, left scale), and the sound velocity $\Delta v/v$, in the c_{11} and c_{33} acoustic modes (up and down red triangles, respectively, right scale). The neutron diffraction intensity is reproduced from Ref. [47]. The sound velocity in the c_{11} mode is divided by a factor of 4.5. The sound velocity measurements presented here are taken at $T\leqslant 4$ K in field-cooled conditions. The dashed line is a guide to the eye.

on polycrystals. Earlier ultrasound studies suggested that this behavior can be caused by LTT distortions [13,71]. On the other hand, anelastic experiments implied a coupling between strain and AFM glass domain wall motion [72]. Those studies are discussed in greater details in Appendix C.

Here we propose an alternative mechanism that could cause the low temperature stiffening in the c_{11} mode. We start by noticing that a stiffening is also observed in the c_{33} mode for $T\lesssim T_\alpha$ (see Fig. 1). As shown in Fig. 7, the low temperature increase of the sound velocity in both the c_{11} and c_{33} modes has a field dependence that scales with the increase in μ^2, the ordered moment squared inferred from neutron diffraction experiment, as discussed previously [13,17]. This scaling can be explained by invoking a biquadratic coupling $F_c=\lambda\epsilon^2M^2$ with M the magnetization, and λ a coupling constant. Note that F_c is symmetry-allowed for all elastic constants of Table I. This coupling produces $\Delta v/v\propto\lambda M^2$ and can naturally account for the experimental observations if we assume that the coupling constant λ is larger for longitudinal modes (c_{11} and c_{33}) than it is for transverse modes [c_{44} and $(c_{11}-c_{12})/2$].

VI. SUMMARY

In summary, we studied sound velocity and attenuation in $La_{1.88}Sr_{0.12}CuO_4$ in high magnetic field. The behavior of the c_{11} and $(c_{11}-c_{12})/2$ elastic constants is highly anomalous. By comparing the anomalies with ^{139}La NMR $1/T_1$ we confirm that they originate from the AFM glass phase via a magnetoacoustic coupling. A semiquantitative analysis of this contribution is made based on a phenomenological model of spin glass systems. Our ultrasound data points toward a strong competition between spin freezing and superconductivity in high magnetic field. A symmetry analysis reveals that the slowing down of spin fluctuations could be associated with a growing nematic susceptibility.

ACKNOWLEDGMENTS

We thank A. Böhmer, I. Paul, and D. Campbell for fruitful discussions, as well as D. Destraz and O. Ivashko for their assistance with sample preparation. Part of this work was performed at the LNCMI, a member of the European Magnetic Field Laboratory (EMFL). Work at the LNCMI was supported by the Laboratoire d'Excellence LANEF (ANR-10-LABX-51-01), French Agence Nationale de la Recherche (ANR) Grant No. ANR-19-CE30-0019-01 (Neptun) and EUR Grant NanoX n°ANR-17-EURE-0009. Work in Zürich was supported by the Swiss National Science Foundation.

APPENDIX A: VORTEX LATTICE CONTRIBUTION TO THE ULTRASOUND PROPERTIES

In our experiments with $H\parallel[001]$, the c_{11} acoustic mode probes the compression modulus of the vortex lattice (VL), whereas $(c_{11}-c_{12})/2$ probes its shear modulus. This last is notorious for its small value, beyond our resolution. On the other hand, the compression modulus of the VL should make a detectable contribution. This contribution should give a step-like increase of the sound velocity and an attenuation peak when decreasing temperature through the depinning transition of the vortex lattice. Both these features should move to lower temperatures with increasing field and disappear for $H\geqslant H_{c2}$.

In Figs. 2(a) and 2(b) there is no evidence of the vortex lattice depinning transition. It has a negligible contribution to the longitudinal sound velocity in LSCO $p=0.12$. This is due to the low value of the irreversibility field, and presumably also

because of the two-dimensional and disordered character of the VL at this doping level [73]. Consequently no signature of the vortex lattice depinning transition is observed in Figs. 2(a) and 2(b) and Fig. 3.

APPENDIX B: IMPACT OF SUPERCONDUCTIVITY ON THE ULTRASOUND PROPERTIES

We discuss the effect of superconductivity on the ultrasound properties which is best observed at low fields. Below 5 T or so, $T_{\min}$ coincides with T_c in both c_{11} and $(c_{11}-c_{12})/2$ in our LSCO $p=0.12$ sample (see Figs. 1 and 2). This behavior has also been observed in LSCO $p\approx 0.14$ up to 14 T by Nohara and coworkers [12]. In this field range $T_{\min}$ appears to be primarily set by superconductivity.

In LSCO, superconductivity can induce an increase of the sound velocity for $T<T_c$ via two mechanisms. First, the superconducting order parameter has a direct coupling with the lattice for $T<T_c$. In cuprates, this coupling produces a hardening in the superconducting state, for both longitudinal and transverse modes [21]. Consequently, an upturn can occur at T_c in both $(c_{11}-c_{12})/2$ and c_{11}. The second possible mechanism is indirect, and involves the competition between superconductivity and magnetism. In zero and low fields, the growth $\chi_4(\omega=0,T)$, signaled by the softening of the sound velocity, can be tempered by the onset of superconductivity. If $\chi_4(\omega=0,T)$ is sufficiently modified through T_c, it can result in an upturn at T_c. As a result of these two possible mechanisms, at zero and low magnetic field, we observe $T_{\min}=T_c$, and $T_{\min}$ decreases as field increases.

However, for $\mu_0 H \geqslant 5\,\mathrm{T}$, $T_{\min}$ increases with magnetic field, meaning that the mechanism causing the softening for $T>T_{\min}$ and the hardening for $T<T_{\min}$ observed for $\mu_0 H \geqslant 5\,\mathrm{T}$ in LSCO $p=0.12$ does not involve the coupling of the superconducting order parameter to the lattice. Increasing the magnetic field above $\mu_0 H=14\,\mathrm{T}$ at $p\approx 0.14$ leads to the same observation [18]. As field increases the superconducting contribution to the sound velocity becomes weaker and the spin freezing contribution larger. For $\mu_0 H \geqslant 5\,\mathrm{T}$ the superconducting contribution is dwarfed by the contribution from the magnetic slowing down. This explains why the difference between $T_{\min}$ and $T_\alpha=T_f$ is large and strongly field dependent for $\mu_0 H<5\,\mathrm{T}$, while smaller and constant for higher fields [see Fig. 2(c)].

The temperature scale T_α is insensitive to a direct contribution from superconductivity. While in conventional superconductors, the opening of the superconducting gap causes an attenuation drop, there is no corresponding behavior in LSCO $p\approx 0.12$. However, $\Delta\alpha(T)$ can be indirectly impacted by the onset of superconductivity at low field because the later modifies the spin dynamics that controls $\Delta\alpha(T)$. This is best illustrated by the zero field $\Delta\alpha(T)$ that shows a remarkable kink at T_c and then a maximum at $T_\alpha\simeq 9.5\,\mathrm{K}$ [see Fig. 2(b)]. Within the dynamical susceptibility model, the ultrasound attenuation is mostly governed by the energy scale E_0 entering τ_4 as indicated by Eq. (4). The kink anomaly at T_c in $\Delta\alpha(T)$ in zero field can be interpreted as a decrease of E_0 for $T<T_c$ caused by the onset of superconductivity.

Because the dynamical susceptibility model does not take into account the impact of superconductivity on spin dynamics, we use an alternative scheme in order to extract E_0 for $\mu_0 H<5\,\mathrm{T}$. At $T=T_\alpha$, the condition $\omega\tau_4(T)=1$ is met. Solving Eq. (6) for E_0 at $T=T_\alpha$ hence yields $E_0=-T_\alpha/\ln(\omega\tau_\infty)$ [43]. In Fig. 8 we compare this T_α derived E_0 with E_0 of Fig. 5(c) obtained with the parametrization of the ultrasound data. Good agreement is found between the two estimations of E_0. As seen in Fig. 8, $-T_\alpha/\ln(\omega\tau_\infty)$ decreases rapidly at low fields, dropping from $E_0\sim 150K$ for $\mu_0 H=5\,\mathrm{T}$ to $E_0=92\,\mathrm{K}$ for $H=0$. This rapid drop reflects the competition between spin freezing and superconductivity.

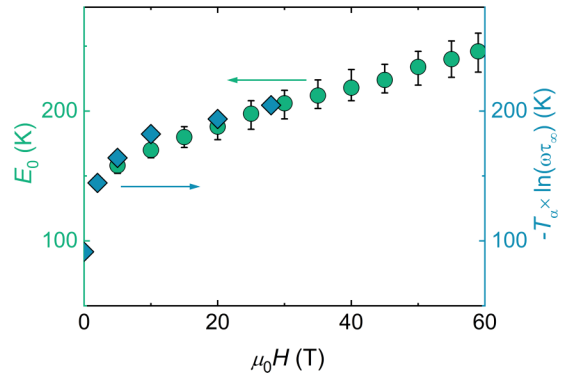

FIG. 8. Comparison between the E_0 energy scale (circles, left scale) extracted from the fitting procedure of Fig. 5 and $-T_\alpha \times \ln(\omega\tau_\infty)$ (diamonds, right scale) determined directly from the data shown in Fig. 2(b), $\omega=2\pi\times 110\,\mathrm{MHz}$ and $\tau_\infty\approx 10^{-13}\,\mathrm{s}$. The energy scale $-T_\alpha\times\ln(\omega\tau_\infty)$ corresponds to an experimental determination of E_0 solely based on T_α, using the condition $\omega\tau_4(T_\alpha)=1$ in Eq. (6) (see text). The rapid drop of $-T_\alpha\times\ln(\omega\tau_\infty)$ at low H is most likely due to the impact of superconductivity on the spin dynamics. Error bars on this quantity are smaller than the size of the symbols.

APPENDIX C: PREVIOUS EXPERIMENTS ON POLYCRYSTALS

In Sec. V C we discuss a scenario that would explain the lattice hardening seen mainly in the c_{11} elastic constant at low temperature. Here, we detail previous putative explanations that have been proposed to explain a similar phenomenology from ultrasound and anelastic studies of polycrystalline La-based compounds.

We first consider previous ultrasound experiments. Around $p\approx 0.12$, in several La-based cuprates and, in particular, LSCO [13,14,71,74], the sound velocity of longitudinal waves increases markedly at low temperature while an attenuation peak occurs. This behavior is most likely related to the anomalous hardening of the c_{11} elastic constant, as suggested by the similar temperature scales and field-enhancement. Interestingly, those previous ultrasound studies have shown that the temperature scale of the lattice hardening evolves smoothly from LBCO $p=0.12$ to LSCO $p=0.12$, and correspond to the coincident OMT-LTT and charge-stripe transition in the former [13,71]. Based on these experiments it has been proposed that in LSCO $p\approx 0.12$ the low temperature lattice hardening arises from the parallel development of local and/or fluctuating LTT distortions and charge-stripes. However, in this scenario it is unclear why the lattice hardening is observed only at low temperature—comparable to T_α—

whereas, in LSCO $p \approx 0.12$, LTT-type tilts are found at temperatures as high as $T = 100\,\mathrm{K}$ in electron diffraction experiments [75,76] and LTT-type reflections are observed up to the OMT-HTT transition temperature T_{st} in x-ray diffraction [7].

Now let us consider anelastic experiments in LSCO and LBCO polycrystals. These have shown that the Young modulus increases markedly at low temperature [77]. The elastic energy loss coefficient shows a step-like increase for $T \leqslant T_f$ and a plateau down to the lowest T [72]. Based on a comparison with nuclear quadrupolar resonance (NQR) experiment, as well as the effect of oxygen vacancy, it has been inferred that the anelastic anomalies arise from a strain induced motion of the antiferromagnetic domain walls of the AFM glass phase [72]. In particular, this naturally explains why these anomalies are observed at temperatures of the order of T_α. However, these experiments are performed at much lower frequency than the ultrasound ones (within the kHz range) and thus do not necessarily probe the same relaxation process as ultrasound experiments [41].

[1] J. M. Tranquada, B. J. Sternlieb, J. D. Axe, Y. Nakamura, and S. Uchida, Evidence for stripe correlations of spins and holes in copper oxide superconductors, Nature **375**, 561 (1995).

[2] E. S. Božin, S. J. L. Billinge, G. H. Kwei, and H. Takagi, Charge-stripe ordering from local octahedral tilts: Underdoped and superconducting $La_{2-x}Sr_xCuO_4 (0 < x < 0.30)$, Phys. Rev. B **59**, 4445 (1999).

[3] A. Bianconi, N. L. Saini, A. Lanzara, M. Missori, T. Rossetti, H. Oyanagi, H. Yamaguchi, K. Oka, and T. Ito, Determination of the Local Lattice Distortions in the CuO_2 Plane of $La_{1.85}Sr_{0.15}CuO_4$, Phys. Rev. Lett. **76**, 3412 (1996).

[4] N. L. Saini, A. Lanzara, H. Oyanagi, H. Yamaguchi, K. Oka, T. Ito, and A. Bianconi, Local lattice instability and stripes in the CuO_2 plane of the $La_{1.85}Sr_{0.15}CuO_4$ system by polarized XANES and EXAFS, Phys. Rev. B **55**, 12759 (1997).

[5] V. Thampy, M. P. M. Dean, N. B. Christensen, L. Steinke, Z. Islam, M. Oda, M. Ido, N. Momono, S. B. Wilkins, and J. P. Hill, Rotated stripe order and its competition with superconductivity in $La_{1.88}Sr_{0.12}CuO_4$, Phys. Rev. B **90**, 100510(R) (2014).

[6] T. P. Croft, C. Lester, M. S. Senn, A. Bombardi, and S. M. Hayden, Charge density wave fluctuations in $La_{2-x}Sr_xCuO_4$ and their competition with superconductivity, Phys. Rev. B **89**, 224513 (2014).

[7] N. B. Christensen, J. Chang, J. Larsen, M. Fujita, M. Oda, M. Ido, N. Momono, E. M. Forgan, A. T. Holmes, J. Mesot, M. Huecker, and M. v. Zimmermann, Bulk charge stripe order competing with superconductivity in $La_{2-x}Sr_xCuO_4$ ($x = 0.12$), arXiv:1404.3192.

[8] J. J. Wen, H. Huang, S. J. Lee, H. Jang, J. Knight, Y. S. Lee, M. Fujita, K. M. Suzuki, S. Asano, S. A. Kivelson, C. C. Kao, and J. S. Lee, Observation of two types of charge-density-wave orders in superconducting $La_{2-x}Sr_xCuO_4$, Nat. Commun. **10**, 3269 (2019).

[9] M.-H. Julien, Magnetic order and superconductivity in $La_{2-x}Sr_xCuO_4$: a review, Phys. B: Condens. Matter **329-333**, 693 (2003).

[10] A. T. Rømer, J. Chang, N. B. Christensen, B. M. Andersen, K. Lefmann, L. Mähler, J. Gavilano, R. Gilardi, C. Niedermayer, H. M. Rønnow, A. Schneidewind, P. Link, M. Oda, M. Ido, N. Momono, and J. Mesot, Glassy low-energy spin fluctuations and anisotropy gap in $La_{2-x}Sr_xCuO_4$, Phys. Rev. B **87**, 144513 (2013).

[11] T. Suzuki, T. Goto, K. Chiba, T. Shinoda, T. Fukase, H. Kimura, K. Yamada, M. Ohashi, and Y. Yamaguchi, Observation of modulated magnetic long-range order in $La_{1.88}Sr_{0.12}CuO_4$, Phys. Rev. B **57**, R3229 (1998).

[12] M. Nohara, T. Suzuki, Y. Maeno, T. Fujita, I. Tanaka, and H. Kojima, Interplay between Lattice Softening and High-T_c Superconductivity in $La_{1.86}Sr_{0.14}CuO_4$, Phys. Rev. Lett. **70**, 3447 (1993).

[13] J. F. Qu, Y. Q. Zhang, X. L. Lu, X. Q. Xiang, Y. L. Liao, G. Li, and X. G. Li, Ultrasonic study on magnetic-field-induced stripe order in $La_{1.88-x}Sr_{0.12}Ba_xCuO_4$, Appl. Phys. Lett. **89**, 162508 (2006).

[14] J. Qu, Y. Zhang, X. Xiang, X. Lu, and X. Li, Effect of magnetic field on the charge-stripe phase in $La_{2-x-y}Nd_ySr_xCuO_4$: An ultrasonic attenuation study, Mater. Sci. Eng. A **442**, 216 (2006).

[15] T. Hanaguri, T. Fukase, T. Suzuki, I. Tanaka, and H. Kojima, Elastic anomalies in a $La_{1.85}Sr_{0.15}CuO_4$ single crystal under high magnetic fields, Phys. B: Condens. Matter **194-196**, 1579 (1994).

[16] S. Sakita, T. Suzuki, F. Nakamura, M. Nohara, Y. Maeno, and T. Fujita, Elastic softening in single-crystalline $La_{2-x}Sr_xCuO_4$ around x=1/8, Phys. B: Condens. Matter **219-220**, 216 (1996).

[17] J.-Y. Prieur and J. Joffrin, Ultrasonic velocity variations in $La_{2-x}Sr_xCuO_4$ single crystals, Phys. Status Solidi C **1**, 3061 (2004).

[18] M. Frachet, I. Vinograd, R. Zhou, S. Benhabib, S. Wu, H. Mayaffre, S. Krämer, S. K. Ramakrishna, A. Reyes, J. Debray, T. Kurosawa, N. Momono, M. Oda, S. Komiya, S. Ono, M. Horio, J. Chang, C. Proust, D. LeBoeuf, and M.-H. Julien, Hidden magnetism at the pseudogap critical point of a high temperature superconductor, Nat. Phys. **16**, 1064 (2020).

[19] E. P. Papadakis, Ultrasonic measurement methods, Physical Acoustics **19**, 81 (1990).

[20] B. Luthi, *Physical Acoustics in the Solid State* (Springer, New York, 2005).

[21] M. Nohara, T. Suzuki, Y. Maeno, T. Fujita, I. Tanaka, and H. Kojima, Unconventional lattice stiffening in superconducting $La_{2-x}Sr_xCuO_4$ single crystals, Phys. Rev. B **52**, 570 (1995).

[22] Y. P. Varshni, Temperature dependence of the elastic constants, Phys. Rev. B **2**, 3952 (1970).

[23] F. Gugenberger, C. Meingast, G. Roth, K. Grube, V. Breit, T. Weber, H. Wühl, S. Uchida, and Y. Nakamura, Uniaxial pressure dependence of T_c from high-resolution dilatometry of untwinned $La_{2-x}Sr_xCuO_4$ single crystals, Phys. Rev. B **49**, 13137 (1994).

[24] V. F. Mitrović, M.-H. Julien, C. de Vaulx, M. Horvatić, C. Berthier, T. Suzuki, and K. Yamada, Similar glassy features in the ^{139}La NMR response of pure and disordered $La_{1.88}Sr_{0.12}CuO_4$, Phys. Rev. B **78**, 014504 (2008).

[25] A. W. Hunt, P. M. Singer, A. F. Cederström, and T. Imai, Glassy slowing of stripe modulation in $(La, Eu, Nd)_{2-x}(Sr, Ba)_xCuO_4$: $A^{63}Cu$ and ^{139}La NQR study down to 350 mK, Phys. Rev. B **64**, 134525 (2001).

[26] B. Simovič, P. C. Hammel, M. Hücker, B. Büchner, and A. Revcolevschi, Experimental evidence for a glass forming stripe liquid in the magnetic ground state of $La_{1.65}Eu_{0.2}Sr_{0.15}CuO_4$, Phys. Rev. B **68**, 012415 (2003).

[27] N. J. Curro, P. C. Hammel, B. J. Suh, M. Hücker, B. Büchner, U. Ammerahl, and A. Revcolevschi, Inhomogeneous Low Frequency Spin Dynamics in $La_{1.65}Eu_{0.2}Sr_{0.15}CuO_4$, Phys. Rev. Lett. **85**, 642 (2000).

[28] N. Bloembergen, E. M. Purcell, and R. V. Pound, Relaxation effects in nuclear magnetic resonance absorption, Phys. Rev. **73**, 679 (1948).

[29] S.-H. Baek, A. Erb, and B. Büchner, Low-energy spin dynamics and critical hole concentrations in $La_{2-x}Sr_xCuO_4 (0.07 \leqslant x \leqslant 0.2)$ revealed by ^{139}La and ^{63}Cu nuclear magnetic resonance, Phys. Rev. B **96**, 094519 (2017).

[30] M.-H. Julien, A. Campana, A. Rigamonti, P. Carretta, F. Borsa, P. Kuhns, A. P. Reyes, W. G. Moulton, M. Horvatić, C. Berthier, A. Vietkin, and A. Revcolevschi, Glassy spin freezing and nmr wipeout effect in the high-T_c superconductor $La_{1.90}Sr_{0.10}CuO_4$: critical discussion of the role of stripes, Phys. Rev. B **63**, 144508 (2001).

[31] A. T. Savici, Y. Fudamoto, I. M. Gat, T. Ito, M. I. Larkin, Y. J. Uemura, G. M. Luke, K. M. Kojima, Y. S. Lee, M. A. Kastner, R. J. Birgeneau, and K. Yamada, Muon spin relaxation studies of incommensurate magnetism and superconductivity in stage-4 $La_2CuO_{4.11}$ and $La_{1.88}Sr_{0.12}CuO_4$, Phys. Rev. B **66**, 014524 (2002).

[32] P. Doussineau, A. Levelut, M. Matecki, J. P. Renard, and W. Schön, Acoustic and magnetic studies of an insulating spin glass, Europhys. Lett. **3**, 251 (1987).

[33] T. C. Hsu and J. B. Marston, Measurement of ultrasound velocity in the spin-glass CuMn, J. Appl. Phys. **61**, 2074 (1987).

[34] G. F. Hawkins and R. L. Thomas, Ultrasonic studies of spin glasses: CuMn, J. Appl. Phys. **49**, 1627 (1978).

[35] E. Gaganidze and P. Esquinazi, Temperature dependence of the sound attenuation at the spin glass transition of metallic spin glasses, Czech. J. Phys. **46**, 2227 (1996).

[36] P. Doussineau, A. Levelut, and W. Schön, Acoustic susceptibility of an insulating spin-glass, Z. Phys. B **73**, 89 (1988).

[37] B. Lüthi, T. Moran, and R. Pollina, Sound propagation near magnetic phase transitions, J. Phys. Chem. Solids **31**, 1741 (1970).

[38] U. G. Volkmann, R. Böhmer, A. Loidl, K. Knorr, U. T. Höchli, and S. Haussühl, Dipolar and Quadrupolar Freezing in $(KBr)_{1-x}(KCN)_x$, Phys. Rev. Lett. **56**, 1716 (1986).

[39] S. Wakimoto, S. Ueki, Y. Endoh, and K. Yamada, Systematic study of short-range antiferromagnetic order and the spin-glass state in lightly doped $La_{2-x}Sr_xCuO_4$, Phys. Rev. B **62**, 3547 (2000).

[40] F. C. Chou, N. R. Belk, M. A. Kastner, R. J. Birgeneau, and A. Aharony, Spin-Glass Behavior in $La_{1.96}Sr_{0.04}CuO_4$, Phys. Rev. Lett. **75**, 2204 (1995).

[41] R. S. Markiewicz, F. Cordero, A. Paolone, and R. Cantelli, Cluster spin-glass distribution functions in $La_{2-x}Sr_xCuO_4$, Phys. Rev. B **64**, 054409 (2001).

[42] L. Lundgren, P. Svedlindh, and O. Beckman, Anomalous time dependence of the susceptibility in a Cu(Mn) spin glass, J. Magn. Magn. Mater. **31-34**, 1349 (1983).

[43] I. Vinograd, Ph.D. thesis, Université Grenoble Alpes (2019).

[44] G. B. Teitel'baum, I. M. Abu-Shiekah, O. Bakharev, H. B. Brom, and J. Zaanen, Spin dynamics and ordering of a cuprate stripe antiferromagnet, Phys. Rev. B **63**, 020507(R) (2000).

[45] J. M. Tranquada, N. Ichikawa, and S. Uchida, Glassy nature of stripe ordering in $La_{1.6-x}Nd_{0.4}Sr_xCuO_4$, Phys. Rev. B **59**, 14712 (1999).

[46] B. Keimer, N. Belk, R. J. Birgeneau, A. Cassanho, C. Y. Chen, M. Greven, M. A. Kastner, A. Aharony, Y. Endoh, R. W. Erwin, and G. Shirane, Magnetic excitations in pure, lightly doped, and weakly metallic La_2CuO_4, Phys. Rev. B **46**, 14034 (1992).

[47] J. Chang, C. Niedermayer, R. Gilardi, N. B. Christensen, H. M. Rønnow, D. F. McMorrow, M. Ay, J. Stahn, O. Sobolev, A. Hiess, S. Pailhes, C. Baines, N. Momono, M. Oda, M. Ido, and J. Mesot, Tuning competing orders in $La_{2-x}Sr_xCuO_4$ cuprate superconductors by the application of an external magnetic field, Phys. Rev. B **78**, 104525 (2008).

[48] B. Lake, H. M. Rønnow, N. B. Christensen, G. Aeppli, K. Lefmann, D. F. McMorrow, P. Vorderwisch, P. Smeididl, N. Mangkorntong, T. Sasagawa, M. Nohara, H. Takagi, and T. E. Mason, Antiferromagnetic order induced by an applied magnetic field in a high-temperature superconductor, Nature **415**, 299 (2002).

[49] K. Yamada, C. H. Lee, K. Kurahashi, J. Wada, S. Wakimoto, S. Ueki, H. Kimura, Y. Endoh, S. Hosoya, G. Shirane, R. J. Birgeneau, M. Greven, M. A. Kastner, and Y. J. Kim, Doping dependence of the spatially modulated dynamical spin correlations and the superconducting-transition temperature in $La_{2-x}Sr_xCuO_4$, Phys. Rev. B **57**, 6165 (1998).

[50] M. Fujita, K. Yamada, H. Hiraka, P. M. Gehring, S. H. Lee, S. Wakimoto, and G. Shirane, Static magnetic correlations near the insulating-superconducting phase boundary in $La_{2-x}Sr_xCuO_4$, Phys. Rev. B **65**, 064505 (2002).

[51] S. Wakimoto, R. J. Birgeneau, M. A. Kastner, Y. S. Lee, R. Erwin, P. M. Gehring, S. H. Lee, M. Fujita, K. Yamada, Y. Endoh, K. Hirota, and G. Shirane, Direct observation of a one-dimensional static spin modulation in insulating $La_{1.95}Sr_{0.05}CuO_4$, Phys. Rev. B **61**, 3699 (2000).

[52] W. Rehwald, The study of structural phase transitions by means of ultrasonic experiments, Adv. Phys. **22**, 721 (1973).

[53] L. Tassini, F. Venturini, Q.-M. Zhang, R. Hackl, N. Kikugawa, and T. Fujita, Dynamical Properties of Charged Stripes in $La_{2-x}Sr_xCuO_4$, Phys. Rev. Lett. **95**, 117002 (2005).

[54] Y. Ando, K. Segawa, S. Komiya, and A. N. Lavrov, Electrical Resistivity Anisotropy from Self-Organized One Dimensionality in High-Temperature Superconductors, Phys. Rev. Lett. **88**, 137005 (2002).

[55] J. Choi, Q. Wang, S. Jöhr, N. B. Christensen, J. Küspert, D. Bucher, D. Biscette, M. Hücker, T. Kurosawa, N. Momono, M. Oda, O. Ivashko, M. V. Zimmermann, M. Janoschek, and J. Chang, Disentangling intertwined quantum states in a prototypical cuprate superconductor, arXiv:2009.06967.

[56] S. A. Kivelson, E. Fradkin, and V. J. Emery, Electronic liquid-crystal phases of a doped Mott insulator, Nature **393**, 550 (1998).

[57] O. Cyr-Choinière, R. Daou, F. Laliberté, C. Collignon, S. Badoux, D. LeBoeuf, J. Chang, B. J. Ramshaw, D. A. Bonn,

W. N. Hardy, R. Liang, J.-Q. Yan, J.-G. Cheng, J.-S. Zhou, J. B. Goodenough, S. Pyon, T. Takayama, H. Takagi, N. Doiron-Leyraud, and L. Taillefer, Pseudogap temperature T^* of cuprate superconductors from the Nernst effect, Phys. Rev. B **97**, 064502 (2018).

[58] N. Auvray, B. Loret, S. Benhabib, M. Cazayous, R. D. Zhong, J. Scheeloch, G. D. Gu, A. Forget, D. Colson, P. I, A. Sacuto, and Y. Gallais, Nematic fluctuations in the cuprate superconductor $Bi_2Sr_2CaCu_2O_{8+\delta}$, Nat. Commun. **10**, 5209 (2019).

[59] A. Arsenault, S. K. Takahashi, T. Imai, W. He, Y. S. Lee, and M. Fujita, ^{139}La NMR investigation of the charge and spin order in a $La_{1.885}Sr_{0.115}CuO_4$ single crystal, Phys. Rev. B **97**, 064511 (2018).

[60] M.-H. Julien, F. Borsa, P. Carretta, M. Horvatić, C. Berthier, and C. T. Lin, Charge Segregation, Cluster Spin Glass, and Superconductivity in $La_{1.94}Sr_{0.06}CuO_4$, Phys. Rev. Lett. **83**, 604 (1999).

[61] S. Katano, M. Sato, K. Yamada, T. Suzuki, and T. Fukase, Enhancement of static antiferromagnetic correlations by magnetic field in a superconductor $La_{2-x}Sr_xCuO_4$ with $x = 0.12$, Phys. Rev. B **62**, R14677 (2000).

[62] A. T. Savici, A. Fukaya, I. M. Gat-Malureanu, T. Ito, P. L. Russo, Y. J. Uemura, C. R. Wiebe, P. P. Kyriakou, G. J. MacDougall, M. T. Rovers, G. M. Luke, K. M. Kojima, M. Goto, S. Uchida, R. Kadono, K. Yamada, S. Tajima, T. Masui, H. Eisaki, N. Kaneko, M. Greven, and G. D. Gu, Muon Spin Relaxation Studies of Magnetic-Field-Induced Effects in High-T_c Superconductors, Phys. Rev. Lett. **95**, 157001 (2005).

[63] B. Khaykovich, S. Wakimoto, R. J. Birgeneau, M. A. Kastner, Y. S. Lee, P. Smeibidl, P. Vorderwisch, and K. Yamada, Field-induced transition between magnetically disordered and ordered phases in underdoped $La_{2-x}Sr_xCuO_4$, Phys. Rev. B **71**, 220508(R) (2005).

[64] J. Chang, A. P. Schnyder, R. Gilardi, H. M. Rønnow, S. Pailhes, N. B. Christensen, C. Niedermayer, D. F. McMorrow, A. Hiess, A. Stunault, M. Enderle, B. Lake, O. Sobolev, N. Momono, M. Oda, M. Ido, C. Mudry, and J. Mesot, Magnetic-Field-Induced Spin Excitations and Renormalized Spin Gap of the Underdoped $La_{1.895}Sr_{0.105}CuO_4$ Superconductor, Phys. Rev. Lett. **98**, 077004 (2007).

[65] G. S. Boebinger, Y. Ando, A. Passner, T. Kimura, M. Okuya, J. Shimoyama, K. Kishio, K. Tamasaku, N. Ichikawa, and S. Uchida, Insulator-to-Metal Crossover in the Normal State of $La_{2-x}Sr_xCuO_4$ Near Optimum Doping, Phys. Rev. Lett. **77**, 5417 (1996).

[66] D. R. Harshman, G. Aeppli, G. P. Espinosa, A. S. Cooper, J. P. Remeika, E. J. Ansaldo, T. M. Riseman, D. L. Williams, D. R. Noakes, B. Ellman, and T. F. Rosenbaum, Freezing of spin and charge in $La_{2-x}Sr_xCuO_4$, Phys. Rev. B **38**, 852 (1988).

[67] S. M. Hayden, G. Aeppli, H. Mook, D. Rytz, M. F. Hundley, and Z. Fisk, Magnetic Fluctuations in $La_{1.95}Ba_{0.05}CuO_4$, Phys. Rev. Lett. **66**, 821 (1991).

[68] I. Watanabe, T. Adachi, S. Yairi, Y. Koike, and K. Nagamine, Change of the dynamics of internal fields in the normal state of $La_{2-x}Sr_xCuO_4$ observed by muon-spin-relaxation, J. Phys. Soc. Jpn. **77**, 124716 (2008).

[69] X. F. Sun, S. Komiya, J. Takeya, and Y. Ando, Magnetic-Field-Induced Localization of Quasiparticles in Underdoped $La_{2-x}Sr_xCuO_4$ Single Crystals, Phys. Rev. Lett. **90**, 117004 (2003).

[70] P. Bourgeois-Hope, S. Y. Li, F. Laliberté, S. Badoux, S. M. Hayden, N. Momono, T. Kurosawa, K. Yamada, H. Takagi, N. Doiron-Leyraud, and L. Taillefer, Link between magnetism and resistivity upturn in cuprates: a thermal conductivity study of $La_{2-x}Sr_xCuO_4$, arXiv:1910.08126.

[71] T. Fukase, T. Hanaguri, T. Nomoto, T. Goto, Y. Koike, S. T., T. Sato, I. Tanaka, and H. Kojima, Ultrasonic and NQR studies of structural phase transitions and superconductivity in $La_{2-x}Sr_xCuO_4$, JJAP series **7**, 213 (1992).

[72] F. Cordero, A. Paolone, R. Cantelli, and M. Ferretti, Anelastic spectroscopy of the cluster spin-glass phase in $La_{2-x}Sr_xCuO_4$, Phys. Rev. B **62**, 5309 (2000).

[73] J. Chang, J. S. White, M. Laver, C. J. Bowell, S. P. Brown, A. T. Holmes, L. Maechler, S. Strässle, R. Gilardi, S. Gerber, T. Kurosawa, N. Momono, M. Oda, M. Ido, O. J. Lipscombe, S. M. Hayden, C. D. Dewhurst, R. Vavrin, J. Gavilano, J. Kohlbrecher, E. M. Forgan, and J. Mesot, Spin density wave induced disordering of the vortex lattice in superconducting $La_{2-x}Sr_xCuO_4$, Phys. Rev. B **85**, 134520 (2012).

[74] T. Goto, T. Suzuki, K. Chiba, T. Shinoda, M. Mori, and T. Fukase, Field-induced spin reorientation and low-temperature structural phase transition in $La_{2-x}Sr_xCuO_4$, Phys. B: Condens. Matter **246-247**, 572 (1998).

[75] Y. Koyama, Y. Wakabayashi, K. Ito, and Y. Inoue, Low-temperature structural transitions and T_c suppression in $La_{2-x}M_xCuO_4$ (M=Ba, Sr), Phys. Rev. B **51**, 9045 (1995).

[76] Y. Horibe, Y. Inoue, and Y. Koyama, Direct observation of dynamic local structure in $La_{2-x}Sr_xCuO_4$ around $x = 0.12$, Phys. Rev. B **61**, 11922 (2000).

[77] F. Cordero, A. Paolone, R. Cantelli, and M. Ferretti, Pinning of the domain walls of the cluster spin-glass phase in the low-temperature-tetragonal phase of $La_{2-x}Ba_xCuO_4$, Phys. Rev. B **64**, 132501 (2001).